

Crystal structure of butenafine hydrochloride, C<sub>23</sub>H<sub>28</sub>NClJames A. Kaduk <sup>1,2,a)</sup> Stacy Gates-Rector <sup>3</sup> and Thomas N. Blanton <sup>3</sup><sup>1</sup>Illinois Institute of Technology, 3101 S. Dearborn St., Chicago, IL 60616, USA<sup>2</sup>North Central College, 131 S. Loomis St., Naperville, IL 60540, USA<sup>3</sup>ICDD, 12 Campus Blvd., Newtown Square, PA 19073-3273, USA

(Received 11 August 2022; accepted 28 November 2022)

The crystal structure of butenafine hydrochloride has been solved and refined using synchrotron X-ray powder diffraction data, and optimized using density functional theory techniques. Butenafine hydrochloride crystallizes in space group  $P2_1$  (#4) with  $a = 13.94807(5)$ ,  $b = 9.10722(2)$ ,  $c = 16.46676(6)$  Å,  $\beta = 93.9663(5)^\circ$ ,  $V = 2086.733(8)$  Å<sup>3</sup>, and  $Z = 4$ . Butenafine hydrochloride occurs as a racemic co-crystal of *R* and *S* enantiomers of the cation. The crystal structure is characterized by parallel stacks of aromatic rings along the *b*-axis. Each cation forms a strong discrete N–H⋯Cl hydrogen bond. The chloride anions also act as acceptors in several C–H⋯Cl hydrogen bonds from methylene, methyl, and aromatic groups. The powder pattern has been submitted to ICDD for inclusion in the Powder Diffraction File™ (PDF®).

© The Author(s), 2023. Published by Cambridge University Press on behalf of International Centre for Diffraction Data. This is an Open Access article, distributed under the terms of the Creative Commons Attribution licence (<http://creativecommons.org/licenses/by/4.0/>), which permits unrestricted re-use, distribution and reproduction, provided the original article is properly cited.

[doi:10.1017/S0885715622000562]

Key words: butenafine, Lotrimin, powder diffraction, Rietveld refinement, density functional theory

## I. INTRODUCTION

Butenafine hydrochloride (sold under the brand names Lotrimin Ultra and Mentax) is the hydrochloride salt form of butenafine, a synthetic benzylamine derivative with fungicidal properties. It is used to treat athlete's foot, ringworm, and jock itch. With extended use, it can have some benefit in treating toenail fungus. The systematic name (CAS Registry Number 101827-46-7) is 1-(4-*tert*-butylphenyl)-*N*-methyl-*N*-(naphthalen-1-ylmethyl)methanamine hydrochloride. A two-dimensional (2D) molecular diagram is shown in Figure 1.

Conformational analyses of both butenafine free base and its protonated cation have been carried out (Mingeot-Leclercq et al., 2001). We are unaware of any published X-ray powder diffraction data on butenafine or butenafine hydrochloride.

This work was carried out as part of a project (Kaduk et al., 2014) to determine the crystal structures of large-volume commercial pharmaceuticals, and include high-quality powder diffraction data for them in the Powder Diffraction File (Gates-Rector and Blanton, 2019).

## II. EXPERIMENTAL

Butenafine hydrochloride was a commercial reagent, purchased from TargetMol (Lot #118887), and was used as-received. The white powder was packed into a 1.5-mm diameter Kapton capillary, and rotated during the measurement at ~50 Hz. The powder pattern was measured at 295 K

at beamline 11-BM (Antao et al., 2008; Lee et al., 2008; Wang et al., 2008) of the Advanced Photon Source at Argonne National Laboratory using a wavelength of 0.458968(2) Å from 0.5 to 50°  $2\theta$  with a step size of 0.001° and a counting time of 0.1 s/step. The high-resolution powder diffraction data were collected using twelve silicon crystal analyzers that allow for high angular resolution, high precision, and accurate peak positions. A silicon (NIST SRM 640c) and alumina (SRM 676a) standard (ratio Al<sub>2</sub>O<sub>3</sub>:Si = 2:1 by weight) was used to calibrate the instrument and refine the monochromatic wavelength used in the experiment.

The pattern was indexed using both JADE Pro (MDI, 2022) and N-TREOR (Altomare et al., 2013) on a primitive monoclinic unit cell with  $a = 13.92505$ ,  $b = 9.09245$ ,  $c = 16.43938$  Å,  $\beta = 93.97^\circ$ ,  $V = 2076.45$  Å<sup>3</sup>, and  $Z = 4$ . A reduced cell search in the Cambridge Structural Database (Groom et al., 2016) yielded 8 hits, but no structures of butenafine derivatives. The suggested space group was  $P2_1$ , which was confirmed by successful solution and refinement of the structure.

A butenafine molecule was downloaded from PubChem (Kim et al., 2019) as Conformer3D\_CID\_2484.sdf. It was converted to a \*.mol2 file using Mercury (Macrae et al., 2020) and into a Fenske-Hall Z-matrix using OpenBabel (O'Boyle et al., 2011). The structure was solved by Monte Carlo simulated annealing techniques as implemented in EXPO2014 (Altomare et al., 2013) using two butenafine molecules and two Cl atoms as fragments. Hydrogen atoms were added to the two N atoms using Materials Studio (Dassault, 2021).

An initial refinement of 181 variables using 18,073 observations and 126 restraints yielded the residuals  $R_{wp} = 0.1378$

<sup>a)</sup> Author to whom correspondence should be addressed. Electronic mail: [kaduk@polycrystallography.com](mailto:kaduk@polycrystallography.com)

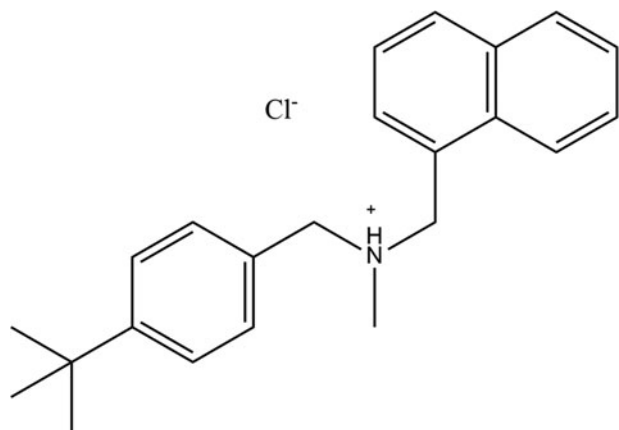


Figure 1. The 2D molecular structure of racemic butenafine hydrochloride.

and  $GOF = 2.49$  (Figure 2). Although the root-mean-square (rms) Cartesian displacement between the Rietveld-refined and DFT-optimized structures of cations 1 and 2 (0.106 and 0.196 Å, respectively; Figures 3 and 4) is within the normal range for correct structures (van de Streek and Neumann, 2014), the Rietveld fit is not as good as one might hope and the structure is chemically unsatisfactory. Only one of the cations (cation 1; the lower atom numbers) forms the expected N–H...Cl hydrogen bond; the N1...Cl104 distance was 3.061 Å (Figure 5). The corresponding N52...Cl103 distance for cation 2 was 3.619 Å. The conformational study of Mingeot-Leclercq et al. (2001) noted that, although the butenafine free base molecule is achiral, protonation can result in both *R* and *S* enantiomers. Both molecules were in the *R* configuration, as they were generated from two copies of the downloaded molecule. Manually inverting the configuration

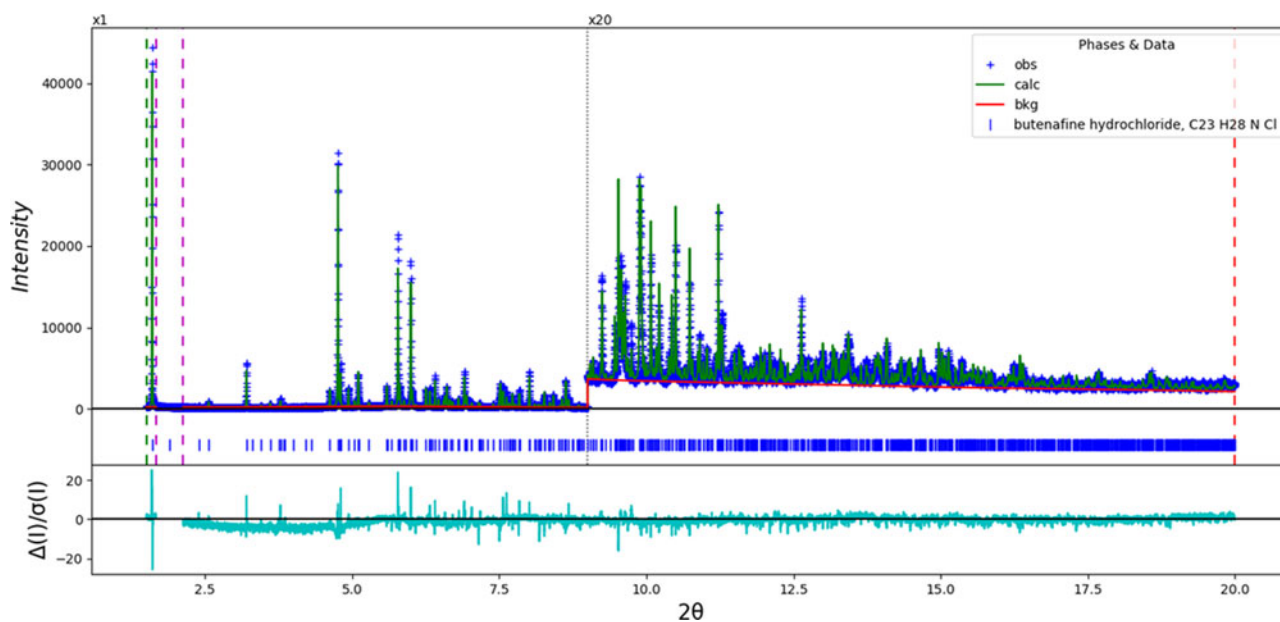


Figure 2. The Rietveld plot for the first (incorrect) refinement of butenafine hydrochloride. The blue crosses represent the observed data points, and the green line is the calculated pattern. The cyan curve is the normalized error plot. The red curve indicates the background. The vertical scale has been multiplied by a factor of 20x for  $2\theta > 9.0^\circ$ . The row of blue tick marks indicates the calculated reflection positions.

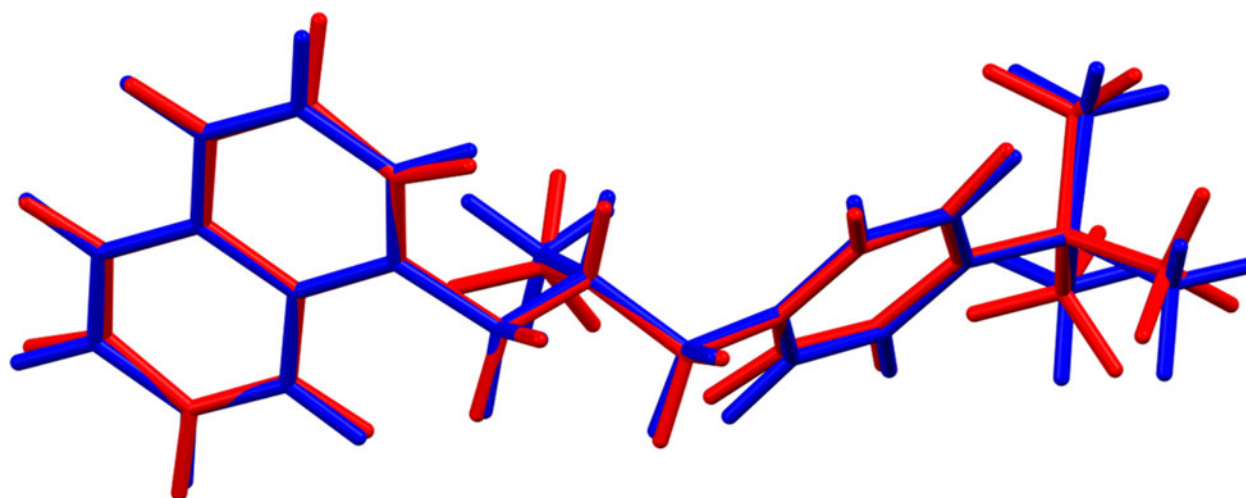


Figure 3. Comparison of the Rietveld-refined (red) and VASP-optimized (blue) structures of cation 1 in butenafine hydrochloride from the first (incorrect) refinement. The rms Cartesian displacement is 0.106 Å. Image generated using Mercury (Macrae et al., 2020).

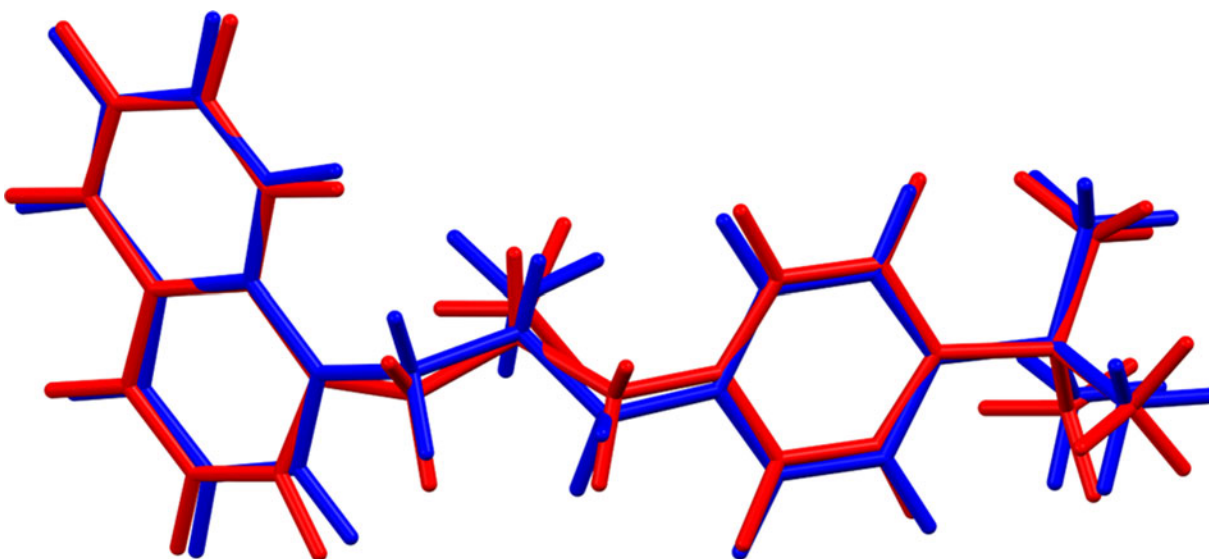


Figure 4. Comparison of the Rietveld-refined (red) and VASP-optimized (blue) structures of cation 2 in butenafine hydrochloride from the first (incorrect) refinement. The rms Cartesian displacement is 0.196 Å. Image generated using Mercury (Macrae et al., 2020).

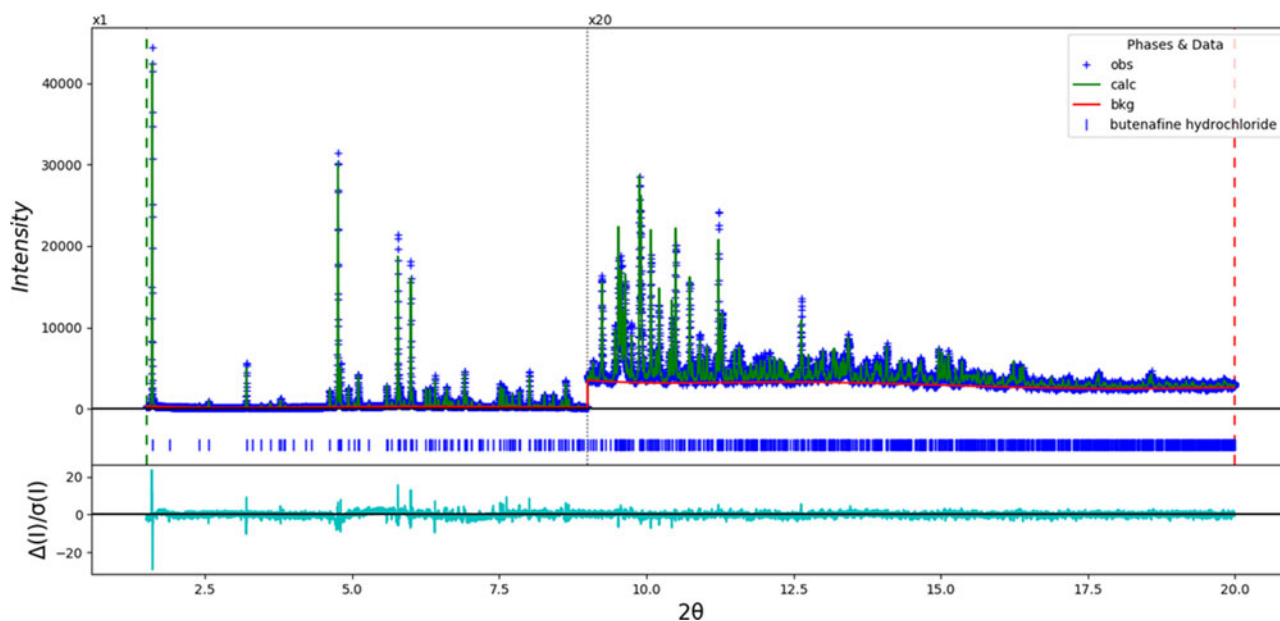


Figure 5. The Rietveld plot for the final refinement of butenafine hydrochloride. The blue crosses represent the observed data points, and the green line is the calculated pattern. The cyan curve is the normalized error plot. The red curve indicates the background. The vertical scale has been multiplied by a factor of 20× for  $2\theta > 9.0^\circ$ . The row of blue tick marks indicates the calculated reflection positions.

of N52 from *R* to *S* using Materials Studio and performing a molecular mechanics-based structure optimization using the Forcite module yielded the initial model for a much more satisfactory Rietveld refinement. Butenafine hydrochloride turns out to crystallize as a racemic co-crystal of enantiomers, explaining the *Z'* value of 2.

Rietveld refinement was carried out using GSAS-II (Toby and Von Dreele, 2013). Only the  $1.5\text{--}20.0^\circ$  portion of the pattern was included in the refinement ( $d_{\min} = 1.321 \text{ \AA}$ ). The *y*-coordinate of N1 was fixed to define the origin. All non-H bond distances and angles were subjected to restraints, based on a Mercury/Mogul Geometry Check (Bruno et al., 2004; Sykes et al., 2011). The Mogul average and standard deviation for each quantity were used as the restraint parameters. The

restraints contributed 1.9% to the final  $\chi^2$ . The hydrogen atoms were included in calculated positions, which were recalculated during the refinement using Materials Studio (Dassault, 2021). The  $U_{\text{iso}}$  of the heavy atoms were grouped by chemical similarity. The  $U_{\text{iso}}$  for the H atoms were fixed at  $1.2\times$  the  $U_{\text{iso}}$  of the heavy atoms to which they are attached. The peak profiles were described using the generalized micro-strain model. The background was modeled using a 6-term shifted Chebyshev polynomial, and a peak at  $5.42^\circ 2\theta$  to model the scattering from the Kapton capillary and any amorphous component.

The final refinement of 168 variables using 18,530 observations and 126 restraints yielded the residuals  $R_{\text{wp}} = 0.0814$  and  $\text{GOF} = 1.45$ . The largest peak ( $0.12 \text{ \AA}$  from C1103) and

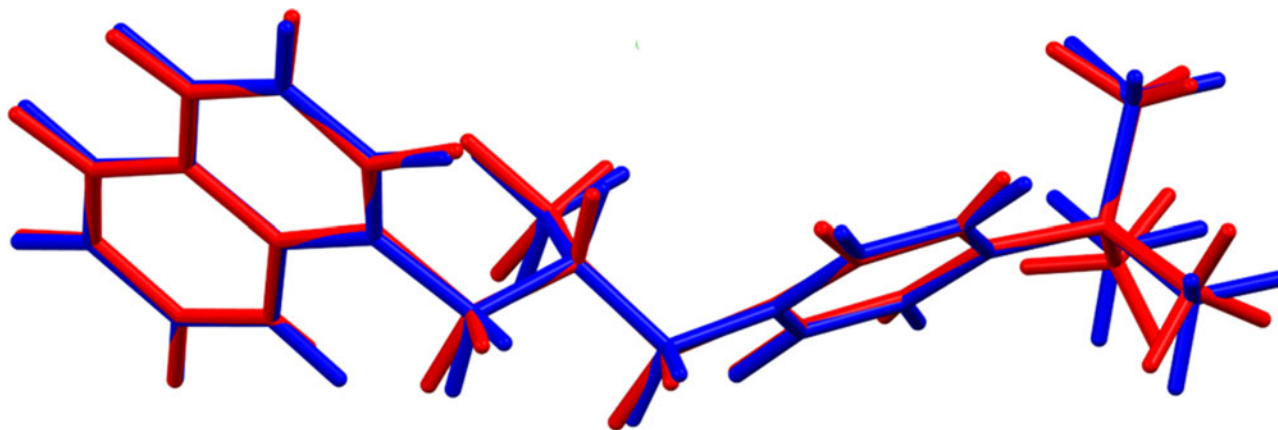


Figure 6. Comparison of the Rietveld-refined (red) and VASP-optimized (blue) structures of cation 1 in butenafine hydrochloride from the final refinement. The rms Cartesian displacement is 0.068 Å. Image generated using Mercury (Macrae et al., 2020).

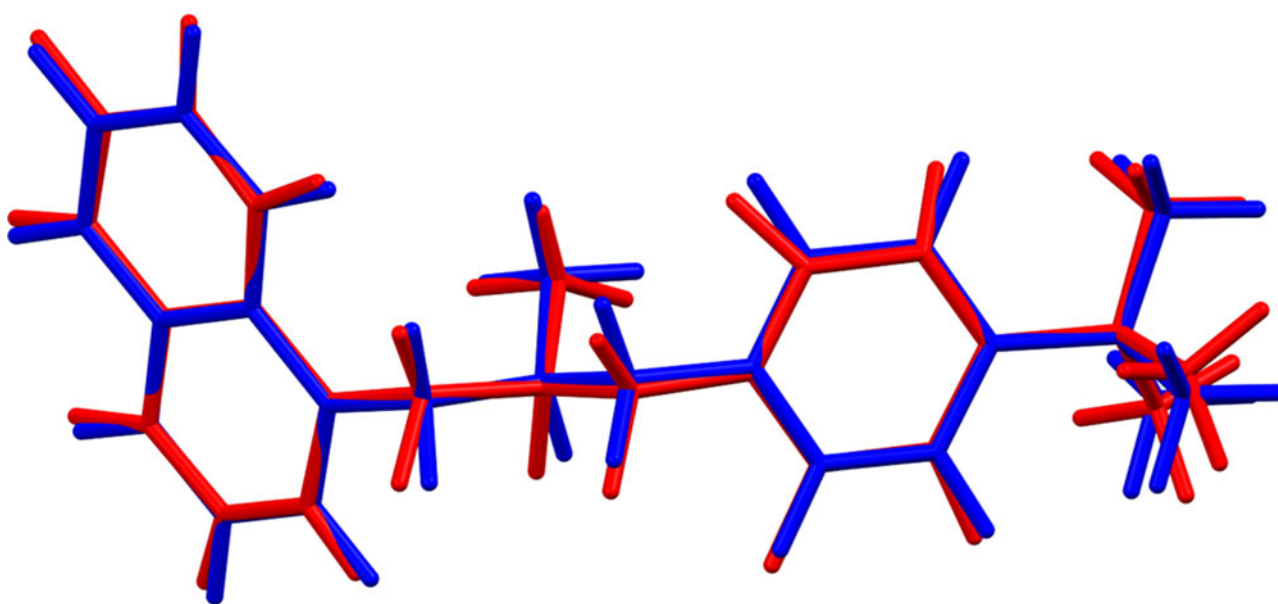


Figure 7. Comparison of the Rietveld-refined (red) and VASP-optimized (blue) structures of cation 2 in butenafine hydrochloride from the final refinement. The rms Cartesian displacement is 0.122 Å. Image generated using Mercury (Macrae et al., 2020).

hole (2.12 Å from C73) in the difference Fourier map were 0.20(4) and  $-0.16(4) e\text{\AA}^{-3}$ , respectively. The largest errors in the difference plot (Figure 5) are in the shapes of some of the low-angle peaks.

The crystal structure was optimized using VASP (Kresse and Furthmüller, 1996) (fixed experimental unit cell) through the MedeA graphical interface (Materials Design, 2016). The calculation was carried out on 16 2.4 GHz processors (each with 4 GB RAM) of a 64-processor HP Proliant DL580 Generation 7 Linux cluster at North Central College. The calculation used the GGA-PBE functional, a plane wave cutoff energy of 400.0 eV, and a  $k$ -point spacing of  $0.5 \text{\AA}^{-1}$  leading to a  $1 \times 2 \times 1$  mesh, and took  $\sim 18.5$  h. A single-point density functional calculation (fixed experimental cell) and population analysis were carried out using CRYSTAL17 (Dovesi et al., 2018). The basis sets for the H, C, N, and O atoms in the calculation were those of Gatti et al. (1994), and that for Cl was that of Peintinger et al. (2013). The calculations were run on a 3.5 GHz PC using 8  $k$ -points and the B3LYP functional, and

took  $\sim 7.5$  h. A Hirshfeld surface analysis was carried out using *CrystalExplorer17* (Turner et al., 2017).

### III. RESULTS AND DISCUSSION

Butenafine hydrochloride occurs as a racemic co-crystal of equal numbers of the *R*- and *S*-enantiomers of the protonated butenafine cation. The rms Cartesian displacements between the Rietveld-refined and DFT-optimized structures of cations 1 and 2 are 0.068 and 0.122 Å (Figures 6 and 7), respectively. The excellent agreement is strong evidence that the structure is correct (van de Streek and Neumann, 2014). This discussion concentrates on the DFT-optimized structure. The asymmetric unit (with atom numbering) is illustrated in Figure 8. The displacement coefficients of the atoms in the *t*-butyl groups of both cations are larger than those of the other atoms, suggesting the possibility of disorder. Since the DFT calculation required an ordered model, we did not attempt to model any disorder. The crystal structure

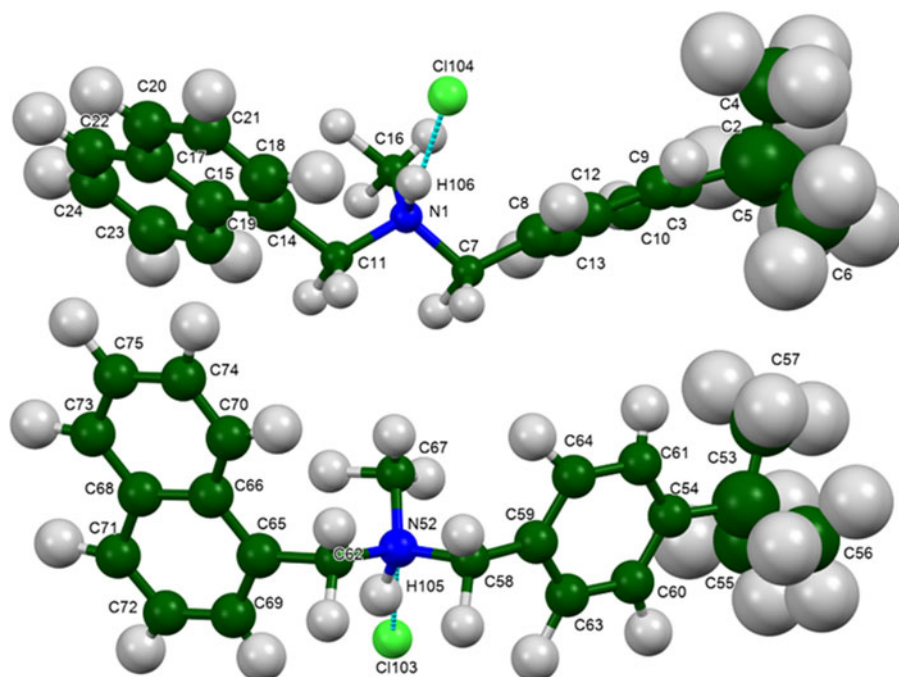


Figure 8. The asymmetric unit of butenafine hydrochloride, with the atom numbering. The atoms are represented by 50% probability spheroids/ellipsoids. Image generated using Mercury (Macrae et al., 2020).

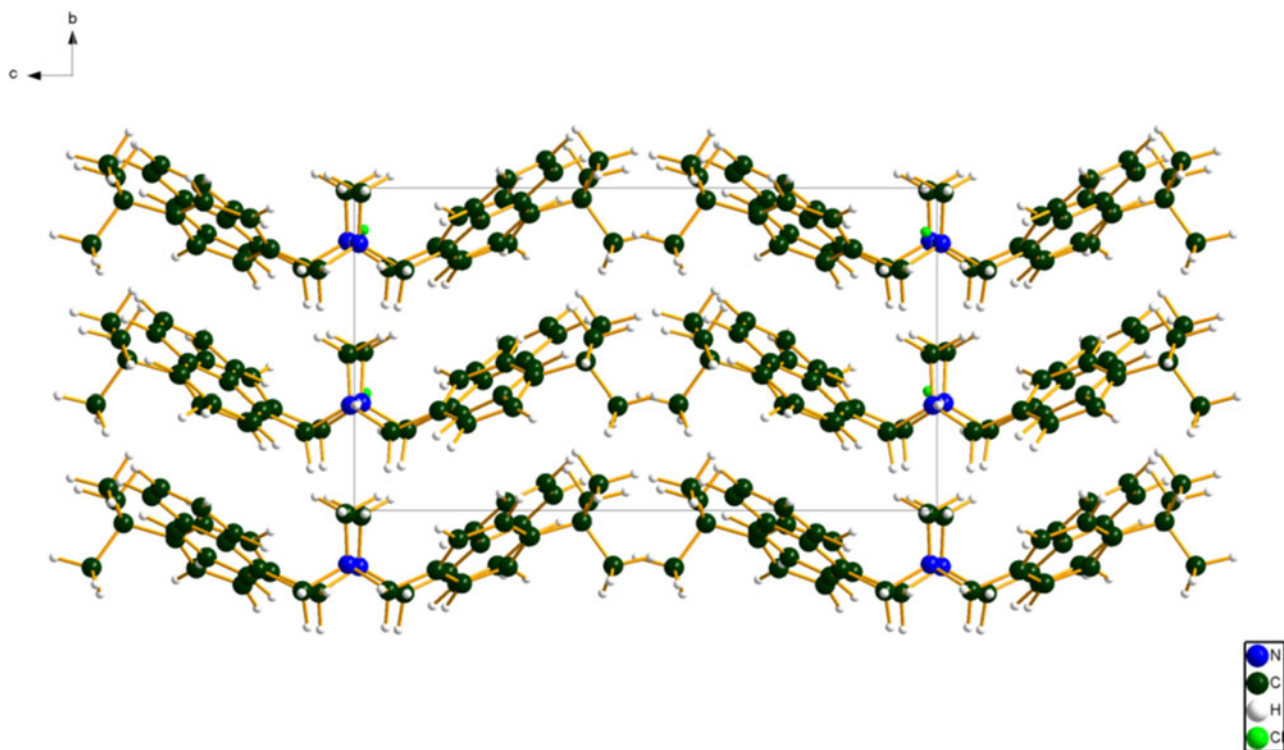


Figure 9. The crystal structure of butenafine hydrochloride, viewed down the *a*-axis. Image generated using Diamond (Crystal Impact, 2022).

(Figure 9) is characterized by parallel stacks of aromatic rings along the *b*-axis. The approximate planes of the naphthalene rings are  $(-1\ 2\ 2)$  and  $(1\ 2\ 2)$ , and those of the phenyl rings are  $(-3\ 3\ 2)$  and  $(1\ 1\ -1)$ .

All of the bond distances, bond angles, and torsion angles fall within the normal ranges indicated by a Mercury/Mogul

Geometry check (Macrae et al., 2020). Quantum chemical geometry optimization of the butenafine cations (DFT/B3LYP/6-31G\*/water) using Spartan '18 (Wavefunction, 2020) indicated that (as expected) the two cations are identical in energy. A conformational analysis (MMFF force field) indicates that the global minimum-energy conformation curls on

TABLE I. Hydrogen bonds (CRYSTAL17) in butenafine hydrochloride.

H-Bond	D-H (Å)	H...A (Å)	D...A (Å)	D-H...A (°)	Overlap ( <i>e</i> )
N52–H105...Cl103	1.077	1.992	3.060	170.6	0.111
N1–H106...Cl104	1.076	1.986	3.053	170.3	0.112
C11–H36...Cl104	1.102	2.611	3.654	157.4	0.037
C62–H87...Cl103	1.102	2.688	3.704	152.9	0.033
C58–H86...Cl103	1.101	2.714	3.749	156.3	0.031
C58–H85...Cl104	1.102	2.670	3.701	155.6	0.030
C7–H34...Cl103	1.101	2.676	3.696	153.7	0.029
C7–H35...Cl104	1.101	2.781	3.794	152.8	0.027
C62–H88...Cl104	1.098	2.995	3.943	144.8	0.013
C70–H97...Cl104	1.093	2.673	3.734	163.5	0.031
C19–H46...Cl103	1.093	2.807	3.872	164.6	0.027
C69–H96...Cl103	1.091	2.977	3.631	118.8	0.012
C13–H41...Cl103	1.094	3.174	4.117	144.8	0.012
C18–H45...Cl104	1.090	3.001	3.570	112.9	0.010
C16–H43...Cl103	1.097	2.713	3.716	151.7	0.026
C67–H95...Cl104	1.097	2.762	3.755	150.3	0.024
C67–H93...C65	1.094	2.606 <sup>a</sup>	2.986	99.3	0.010

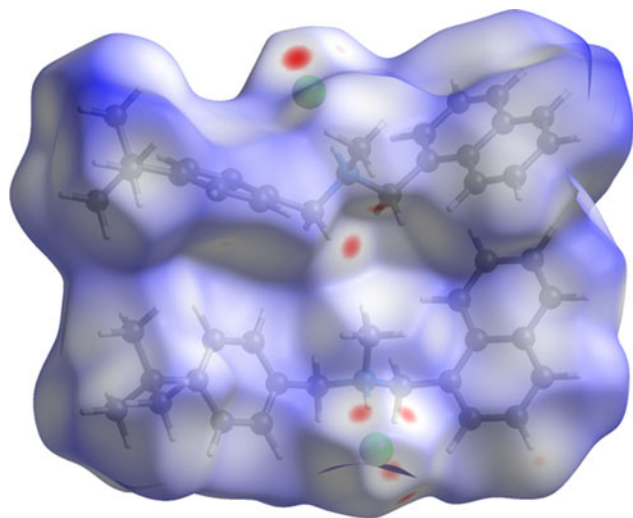
<sup>a</sup>Intramolecular.

Figure 10. The Hirshfeld surface of butenafine hydrochloride. Intermolecular contacts longer than the sums of the van der Waals radii are colored blue, and contacts shorter than the sums of the radii are colored red. Contacts equal to the sums of radii are white. Image generated using CrystalExplorer (Turner et al., 2017).

itself to form an intramolecular (naphthalene) C–H...phenyl hydrogen bond. Cation–anion and cation–cation interactions are thus important in determining the solid-state conformation.

Analysis of the contributions to the total crystal energy of the structure using the Forcite module of Materials Studio (Dassault, 2021) suggests that the intramolecular deformation energy is dominated by bond and angle distortion terms, as might be expected for fused ring systems. The intermolecular energy is dominated by electrostatic attractions, which in this force field analysis include hydrogen bonds. The hydrogen bonds are better analyzed using the results of the DFT calculation.

As expected, each cation forms a strong discrete N–H...Cl hydrogen bond (Table I). The chloride anions also act as acceptors in several C–H...Cl hydrogen bonds from methylene, methyl, and aromatic groups.

The volume enclosed by the Hirshfeld surface of butenafine hydrochloride (Figure 10, Hirshfeld, 1977; Turner et al., 2017) is 1033.08 Å<sup>3</sup>, 99.01% of ½ the unit cell volume. The packing density is thus higher than normal. The only significant close contacts (red in Figure 10) involve the hydrogen bonds. The volume/non-hydrogen atom is larger than normal at 20.9 Å<sup>3</sup>.

The Bravais–Friedel–Donnay–Harker (Bravais, 1866; Friedel, 1907; Donnay and Harker, 1937) morphology suggests that we might expect an elongated morphology for butenafine hydrochloride, with ⟨010⟩ as the principal axis. A second-order spherical harmonic preferred orientation model was included in the refinement. The texture index was 1.007(0), indicating that preferred orientation was not significant for this rotated capillary specimen. The powder pattern of butenafine hydrochloride from this synchrotron data set has been submitted to ICDD for inclusion in the Powder Diffraction File.

#### IV. DEPOSITED DATA

The Crystallographic Information Framework (CIF) files containing the results of the Rietveld refinement (including the raw data) and the DFT geometry optimization were deposited with the ICDD. The data can be requested at [info@icdd.com](mailto:info@icdd.com).

#### ACKNOWLEDGMENTS

The use of the Advanced Photon Source at Argonne National Laboratory was supported by the U.S. Department of Energy, Office of Science, Office of Basic Energy Sciences, under Contract No. DE-AC02-06CH11357. This work was partially supported by the International Centre for Diffraction Data. We thank Lynn Ribaud and Saul Lapidus for their assistance in the data collection.

#### CONFLICTS OF INTEREST

The authors have no conflicts of interest to declare.

## REFERENCES

- Altomare, A., C. Cuocci, C. Giacobozzo, A. Moliterni, R. Rizzi, N. Corriero, and A. Falcicchio. 2013. "EXPO2013: A Kit of Tools for Phasing Crystal Structures from Powder Data." *Journal of Applied Crystallography* 46: 1231–5.
- Antao, S. M., I. Hassan, J. Wang, P. L. Lee, and B. H. Toby. 2008. "State-of-the-Art High-Resolution Powder X-Ray Diffraction (HRPXR) Illustrated with Rietveld Refinement of Quartz, Sodalite, Tremolite, and Meionite." *Canadian Mineralogist* 46: 1501–9.
- Bravais, A. 1866. *Etudes Cristallographiques*. Paris, Gauthier Villars.
- Bruno, I. J., J. C. Cole, M. Kessler, J. Luo, W. D. S. Motherwell, L. H. Purkis, B. R. Smith, R. Taylor, R. I. Cooper, S. E. Harris, and A. G. Orpen. 2004. "Retrieval of Crystallographically-Derived Molecular Geometry Information." *Journal of Chemical Information and Computer Sciences* 44: 2133–44.
- Crystal Impact. 2022. *Diamond – Crystal and Molecular Structure Visualization*. Bonn, Germany, Crystal Impact – Dr. H. Putz & Dr. K. Brandenburg. <https://www.crystalimpact.de/diamond>.
- Dassault Systèmes. 2021. *Materials Studio 2021*. San Diego, CA, BIOVIA.
- Donnay, J. D. H., and D. Harker. 1937. "A New Law of Crystal Morphology Extending the Law of Bravais." *American Mineralogist* 22: 446–47.
- Dovesi, R., A. Erba, R. Orlando, C. M. Zicovich-Wilson, B. Civalieri, L. Maschio, M. Rerat, S. Casassa, J. Baima, S. Salustro, and B. Kirtman. 2018. "Quantum-Mechanical Condensed Matter Simulations with CRYSTAL." *Wiley Interdisciplinary Reviews: Computational Molecular Science* 8: e1360.
- Friedel, G. 1907. "Etudes sur la loi de Bravais." *Bulletin de la Société française de Minéralogie* 30: 326–455.
- Gates-Rector, S., and T. Blanton. 2019. "The Powder Diffraction File: A Quality Materials Characterization Database." *Powder Diffraction* 39 (4): 352–60.
- Gatti, C., V. R. Saunders, and C. Roetti. 1994. "Crystal-Field Effects on the Topological Properties of the Electron-Density in Molecular Crystals - The Case of Urea." *Journal of Chemical Physics* 101: 10686–96.
- Groom, C. R., I. J. Bruno, M. P. Lightfoot, and S. C. Ward. 2016. "The Cambridge Structural Database." *Acta Crystallographica Section B: Structural Science, Crystal Engineering and Materials* 72: 171–9.
- Hirshfeld, F. L. 1977. "Bonded-Atom Fragments for Describing Molecular Charge Densities." *Theoretica Chimica Acta* 44: 129–38.
- Kaduk, J. A., C. E. Crowder, K. Zhong, T. G. Fawcett, and M. R. Suchomel. 2014. "Crystal Structure of Atomoxetine Hydrochloride (Strattera), C<sub>17</sub>H<sub>22</sub>NOCl." *Powder Diffraction* 29 (3): 269–73.
- Kim, S., J. Chen, T. Cheng, A. Gindulyte, J. He, S. He, Q. Li, B. A. Shoemaker, P. A. Thiessen, B. Yu, L. Zaslavsky, J. Zhang, and E. E. Bolton. 2019. "PubChem 2019 Update: Improved Access to Chemical Data." *Nucleic Acids Research* 47 (D1): D1102–9. doi:10.1093/nar/gky1033.
- Kresse, G., and J. Furthmüller. 1996. "Efficiency of Ab-Initio Total Energy Calculations for Metals and Semiconductors Using a Plane-Wave Basis Set." *Computational Materials Science* 6: 15–50.
- Lee, P. L., D. Shu, M. Ramanathan, C. Preissner, J. Wang, M. A. Beno, R. B. Von Dreele, L. Ribaud, C. Kurtz, S. M. Antao, X. Jiao, and B. H. Toby. 2008. "A Twelve-Analyzer Detector System for High-Resolution Powder Diffraction." *Journal of Synchrotron Radiation* 15 (5): 427–32.
- Macrae, C. F., I. Sovago, S. J. Cottrell, P. T. A. Galek, P. McCabe, E. Pidcock, M. Platings, G. P. Shields, J. S. Stevens, M. Towler, and P. A. Wood. 2020. "Mercury 4.0: From Visualization to Design and Prediction." *Journal of Applied Crystallography* 53: 226–35.
- Materials Design. 2016. *MedeA 2.20.4*. Angel Fire, NM, Materials Design Inc.
- MDI. 2022. *JADE Pro Version 8.2 (Computer Software)*. Livermore, CA, USA, Materials Data.
- Mingeot-Leclercq, M.-P., X. Gallet, C. Flore, F. Van Bembeke, J. Peuvot, and R. Brasseur. 2001. "Experimental and Conformational Analyses of Interactions Between Butenafine and Lipids." *Antimicrobial Agents and Chemotherapy* 45: 3347–54.
- O'Boyle, N., M. Banck, C. A. James, C. Morley, T. Vandermeersch, and G. R. Hutchison. 2011. "Open Babel: An Open Chemical Toolbox." *Journal of Cheminformatics* 3: 33. doi:10.1186/1758-2946-3-33.
- Peintinger, M. F., D. Vilela Oliveira, and T. Bredow. 2013. "Consistent Gaussian Basis Sets of Triple-Zeta Valence with Polarization Quality for Solid-State Calculations." *Journal of Computational Chemistry* 34: 451–9.
- Sykes, R. A., P. McCabe, F. H. Allen, G. M. Battle, I. J. Bruno, and P. A. Wood. 2011. "New Software for Statistical Analysis of Cambridge Structural Database Data." *Journal of Applied Crystallography* 44: 882–6.
- Toby, B. H., and R. B. Von Dreele. 2013. "GSAS II: The Genesis of a Modern Open Source All Purpose Crystallography Software Package." *Journal of Applied Crystallography* 46: 544–9.
- Turner, M. J., J. J. McKinnon, S. K. Wolff, D. J. Grimwood, P. R. Spackman, D. Jayatilaka, & M. A. Spackman. 2017. *CrystalExplorer17*. University of Western Australia. <http://hirshfeldsurface.net>.
- van de Streek, J., and M. A. Neumann. 2014. "Validation of Molecular Crystal Structures from Powder Diffraction Data with Dispersion-Corrected Density Functional Theory (DFT-D)." *Acta Crystallographica Section B: Structural Science, Crystal Engineering and Materials* 70 (6): 1020–32.
- Wang, J., B. H. Toby, P. L. Lee, L. Ribaud, S. M. Antao, C. Kurtz, M. Ramanathan, R. B. Von Dreele, and M. A. Beno. 2008. "A Dedicated Powder Diffraction Beamline at the Advanced Photon Source: Commissioning and Early Operational Results." *Review of Scientific Instruments* 79: 085105.
- Wavefunction, Inc. 2020. *Spartan '18 Version 1.4.5*. Irvine, CA, Wavefunction Inc.